Available online at www.sciencedirect.com
SCIENCE DIRECT®
International Journal of Heat and Fluid Flow 26 (2005) 597–612
International Journal of HEAT AND FLUID FLOW
www.elsevier.com/locate/ijhff

Finite element moving mesh analysis of phase change problems with natural convection

R.T. Tenchev [a,*], J.A. Mackenzie [a], T.J. Scanlon [b], M.T. Stickland [b]

[a] Department of Mathematics, University of Strathclyde, Glasgow G1 1XH, UK
[b] Department of Mechanical Engineering, University of Strathclyde, Glasgow G1 1XJ, UK

Accepted 13 March 2005
Available online 3 June 2005

Abstract

This paper discusses the application of an *r*-refinement, moving mesh technique for the solution of heat transfer problems with natural convection and phase change. The moving mesh technique keeps the number of elements and their connectivity fixed and clusters the nodes towards the phase change front at the expense of the solution of an extra differential equation. The governing differential equations describing the physical problem are modified to account for the mesh movement between time steps. The energy conservation equation uses the apparent heat capacity method to take into account the latent heat of phase change. The finite element discretization of all equations is presented. Several test problems are solved and the moving mesh FEM results are in a very good agreement with those in the published literature. The sensitivity of the results to variations of some user-definable computational parameters is found to be low, which means that the moving mesh method may be used without extensive previous experience. Its basic advantage is that less elements may be used to achieve accurate results.
© 2005 Elsevier Inc. All rights reserved.

Keywords: Moving mesh; Phase change; Natural convection

1. Introduction

Phase change problems (solidification or melting) are also known as Stefan problems or moving boundary problems. Their main characteristic feature is that, in addition to the fixed boundaries of the domain, there is a boundary across which the phase change takes place (Crank, 1984; Ockendon and Hodgkins, 1975). This phase change boundary is time dependent and is not known a priori. Thermodynamic equilibrium conditions are to be satisfied on it. The problems are highly non-linear and analytical solutions do not exist except in some very simple cases. Due to their importance many numerical approximations have been developed to solve these problems (Dalhuijsen and Segal, 1981; Lewis and Roberts, 1987; Pardo and Weckman, 1990; Salcuden and Abdullah, 1988; Thomas et al., 1984), which can be classified in two main categories: front tracking methods and fixed grid methods.

With front tracking methods (Gupta, 2000; Pardo and Weckman, 1990; Voller et al., 1990) the discrete phase change front is tracked continuously and treated as a moving boundary between the liquid and solid phase. Different differential equations may be used in these phases. The latent heat involved in the phase change is treated explicitly (hence accurately) as an internal boundary condition. The change in size and shape of the computational domain requires either grid movement techniques or co-ordinate system transformations. The front tracking method is applicable for problems with isothermal phase change. It is generally not suitable for problems where the phase change takes

* Corresponding author. Tel.: +44 141 548 3668; fax: +44 141 552 8657.
E-mail address: rosen.tenchev@strath.ac.uk (R.T. Tenchev).

0142-727X/$ - see front matter © 2005 Elsevier Inc. All rights reserved.
doi:10.1016/j.ijheatfluidflow.2005.03.003

Nomenclature

G	moving mesh monitor function	μ_1, μ_2	coefficients in G, governing mesh density at the phase change front and at the boundaries
h	latent heat of phase change	ξ, η	computational coordinates in 2D
T_m	phase change temperature	ζ, s	computational and physical coordinates in 1D
β	coefficient of volume expansion	τ	dimensionless time
ε_1, ε_2	lower and upper limits of the phase change temperature interval $\varepsilon = \varepsilon_1 + \varepsilon_2$		

place within a temperature interval and involves the formation of a so called mushy region.

With fixed grid methods (Crivelli and Idelsohn, 1986; Fachinotti et al., 1999; Morgan et al., 1978; Nedjar, 2002; Rolph and Bathe, 1982; Tamma and Namburu, 1990; Voller and Cross, 1981) the phase change front is not tracked explicitly but is instead recovered a posteriori from the computed temperature field. These methods are also known as single domain methods because the same differential equation can be used for the solid and liquid region. Hence, their basic advantage is that the numerical solution can be achieved through simple modifications of existing heat transfer numerical methods. The essential feature, however, is the way the latent heat evolution is treated: either by the use of an apparent heat capacity coefficient or by the use a heat source/sink term. These approaches are collectively known as the enthalpy method, because they can be derived from the energy conservation equation written in terms of the enthalpy, which is the sum of the apparent and latent heat. Enthalpy methods are the natural choice when the phase change occurs over a temperature interval. In the case of isothermal phase change there is a discontinuity in the enthalpy across the phase change front, which is normally smoothed by assuming that the phase change occurs over a temperature interval.

When the apparent heat capacity method is used the heat capacity of the mushy region is increased by a term which is directly proportional to the latent heat and is inversely proportional to the phase change interval. There will be loss of accuracy if a region changes its state from solid to liquid or vice versa without passing through the mushy state. The latter may be avoided by either decreasing the computational time step or increasing the phase change interval. The argument is also valid for the source/sink term formulation.

Enthalpy methods either require a phasewise exact integration strategy (Nigro et al., 2000) or a fine mesh near the phase change front in order to capture the large enthalpy gradient in the mushy region. The smaller the phase change interval the narrower the mushy region is and the more refined the mesh should be. If it is expected that the phase change front will transverse the whole domain then a refined mesh should be used everywhere, although it is required only close to the phase change front, and near domain boundaries to pick up boundary layer effects. This serious disadvantage can be overcome if adaptive mesh refinement is employed. Either an h or r-adaptive strategy could be used for this purpose. One advantage of the r-refinement or moving mesh approach is that the element connectivity usually remains unchanged and hence the code is much easier to implement than an h-refinement code which requires a more complicated data structure. Examples of such moving mesh methods include: (Beckett et al., 2001, 2002; Cao et al., 1999; Huang, 1999; Lynch, 1985; Lynch and O'Neill, 1981; Miller and Miller, 1981; Mackenzie and Robertson, 2000).

The idea behind the moving mesh method is that a local mesh refinement is applied only where and when it is required. The total number of elements and their connectivity stay constant throughout the solution process. A new mesh is generated at every time step. The computed solution from the previous time step (e.g. the phase change isotherm) is used to determine where the mesh should be refined. The method is based on the single domain formulation although the grid is not fixed. The method is not a front tracking one because the moving mesh technique does not ensure that element nodes lie on the phase change isotherm thus tracking it explicitly.

The present paper investigates the application of the moving mesh technique in the finite element solution of two dimensional phase change problems when the apparent heat capacity method is used and the fluid flow is driven by natural convection. Both melting and freezing problems are considered. The sensitivity of the results to the variation of some computational parameters is studied.

2. Governing equations

The governing differential equations are presented in the order they are solved at each time step of the FEM solution. First, the energy equation is solved (using computed velocities from the previous time step), which gives the temperature distribution and the position of the phase change front. Second, the moving mesh equations are solved to adapt the mesh towards the phase

change front. Since the time step and the movement of the front are small there is no need to iterate between the two analyses. Finally, the Navier–Stokes equations are solved to determine the velocity of the fluid due to the natural convection.

2.1. Energy equation

The energy equation for transient heat transfer by both conduction and convection is

$$\frac{\partial(\rho c T)}{\partial t} = \nabla \cdot (k \nabla T) - \nabla \cdot (\rho c T \mathbf{u}) \tag{1}$$

and it should be modified to account for the mesh movement.

When the mesh (i.e. the differential volume for which Eq. (1) is derived) is moving with velocity $\mathrm{d}\mathbf{x}/\mathrm{d}t$ the total time derivative is required:

$$\frac{\mathrm{D}(\rho c T)}{\mathrm{D}t} = \frac{\partial(\rho c T)}{\partial t} + \nabla(\rho c T) \cdot \frac{\mathrm{d}\mathbf{x}}{\mathrm{d}t} \tag{2}$$

The notation $\mathrm{D}(\cdot)/\mathrm{D}t$ means differentiation with respect to time along the grid trajectory $(x(t), y(t))$. If the mesh is fixed $\mathrm{D}(\cdot)/\mathrm{D}t \equiv \partial(\cdot)/\partial t$. Substituting the partial time derivative from Eq. (1) into Eq. (2) and rearranging, results:

$$\frac{\mathrm{D}(\rho c T)}{\mathrm{D}t} = \nabla \cdot (k \nabla T) - \nabla \cdot (\rho c T \mathbf{u}) + \nabla(\rho c T) \cdot \frac{\mathrm{d}\mathbf{x}}{\mathrm{d}t} \tag{3}$$

When the fluid is incompressible ($\nabla \cdot \mathbf{u} = 0$ and $\nabla \cdot (\rho c T \mathbf{u}) = \mathbf{u} \cdot \nabla(\rho c T)$), Eq. (3) can be written as:

$$\frac{\mathrm{D}(\rho c T)}{\mathrm{D}t} = \nabla \cdot (k \nabla T) - \left(\mathbf{u} - \frac{\mathrm{d}\mathbf{x}}{\mathrm{d}t}\right) \cdot \nabla(\rho c T) \tag{4}$$

The above equation can be derived directly from Eq. (1) if the differential volume (i.e. the mesh), which is moving with $\mathrm{d}\mathbf{x}/\mathrm{d}t$, is considered fixed in space and the fluid velocity instead of $\mathbf{u}$ is $\mathbf{u} - \mathrm{d}\mathbf{x}/\mathrm{d}t$.

The phase change is assumed to take place within a temperature interval. The latent heat h is accounted for by using an apparent heat capacity:

$$\rho c = \begin{cases} \rho c_{\text{solid}} & \text{if } T_{\text{m}} - \varepsilon_1 > T \\ \dfrac{\rho c_{\text{solid}} + \rho c_{\text{liquid}}}{2} + \dfrac{\rho h}{\varepsilon_1 + \varepsilon_2} & \text{if } T_{\text{m}} - \varepsilon_1 \leqslant T \leqslant T_{\text{m}} + \varepsilon_2 \\ \rho c_{\text{liquid}} & \text{if } T > T_{\text{m}} + \varepsilon_2 \end{cases} \tag{5}$$

2.1.1. FEM approximation

Galerkin's FEM discretization results in a system of ordinary differential equations:

$$\mathbf{C}_T \frac{\mathrm{D}\mathbf{T}}{\mathrm{D}t} + (\mathbf{K}_T + \mathbf{U}_T)\mathbf{T} = \mathbf{F}_T \tag{6}$$

where $\mathbf{C}_T = \sum \mathbf{C}_T^e$, $\mathbf{K}_T = \sum \mathbf{K}_T^e$, etc. In future, for simplicity, the superscript 'e' will be omitted in all element matrices. Matrices $\mathbf{C}_T$ and $\mathbf{K}_T$ are the same as in the case of a stationary mesh:

$$\mathbf{C}_T = \int\int_\Omega \mathbf{N}^{\mathrm{T}} \rho c \mathbf{N} \, \mathrm{d}\Omega;$$
$$\mathbf{K}_T = \int\int_\Omega k \left(\frac{\partial \mathbf{N}^{\mathrm{T}}}{\partial x} \frac{\partial \mathbf{N}}{\partial x} + \frac{\partial \mathbf{N}^{\mathrm{T}}}{\partial y} \frac{\partial \mathbf{N}}{\partial y} \right) \mathrm{d}\Omega; \tag{7}$$

and $\mathbf{N} = \lfloor N_1 \quad N_2 \quad \cdots \quad N_n \rfloor$ is the row vector of the shape functions for an element with n nodes and are also used as weighting functions. In the present studies four node bi-linear elements are used. For the examples considered later we have found that the convective term is not dominant and there is no need to use upwinded weighting functions. The subscript T is used to indicate matrices and vectors used in the energy equation, i.e. when temperature is computed.

The term in Eq. (3) involving the mesh velocity $\mathrm{d}\mathbf{x}/\mathrm{d}t$ may be treated in two ways. Implicitly, which is the more accurate formulation if the mesh velocity is known at the current mesh configuration and time step. This formulation contributes to $\mathbf{U}_T$:

$$\mathbf{U}_T = \int\int_\Omega \mathbf{N}^{\mathrm{T}} \rho c \left[\left(u - \frac{\mathrm{d}x}{\mathrm{d}t} \right) \frac{\partial \mathbf{N}}{\partial x} + \left(v - \frac{\mathrm{d}y}{\mathrm{d}t} \right) \frac{\partial \mathbf{N}}{\partial y} \right] \mathrm{d}\Omega;$$
$$\mathbf{F}_T = 0 \tag{8a}$$

Explicitly, it will contribute to $\mathbf{F}_T$, using the temperature computed at the previous time step and mesh.

$$\mathbf{U}_T = \int\int_\Omega \mathbf{N}^{\mathrm{T}} \rho c \left(u \frac{\partial \mathbf{N}}{\partial x} + v \frac{\partial \mathbf{N}}{\partial y} \right) \mathrm{d}\Omega;$$
$$\mathbf{F}_T = \int\int_\Omega \mathbf{N}^{\mathrm{T}} \rho c \nabla T^{i-1} \cdot \frac{\mathrm{d}\mathbf{x}}{\mathrm{d}t} \mathrm{d}\Omega \tag{8b}$$

The mesh velocity can be computed only approximately, (i—time, Δt—time step) as:

$$\frac{\mathrm{d}\mathbf{x}}{\mathrm{d}t} \approx \frac{\mathbf{x}^i - \mathbf{x}^{i-1}}{\Delta t}, \tag{9}$$

which may be considered as the averaged velocity at time $i - \frac{1}{2}$. So both implicit and explicit formulations are approximate. In the present study the explicit formulation is used for simplicity. Making use of nodal values and shape functions, the force term in Eq. (8b) is

$$\mathbf{F}_T = \int\int_\Omega \mathbf{N}^{\mathrm{T}} \rho c \left(\left(\frac{\partial N_j}{\partial x^{i-1}} T_j^{i-1} \right) \frac{(N_j x_j^i) - (N_j x_j^{i-1})}{\Delta t} + \left(\frac{\partial N_j}{\partial y^{i-1}} T_j^{i-1} \right) \frac{(N_j y_j^i) - (N_j y_j^{i-1})}{\Delta t} \right) \mathrm{d}\Omega \tag{10}$$

where the superscript i denotes at which time the variable is computed. Repeated index j within the brackets means summation over the element nodes.

The ordinary differential equations, Eq. (6), are discretized by the backwards Euler method (i.e. the θ method, with $\theta = 1$). The additional advantage, compared to other methods with $\theta = 1/2$ or $\theta = 3/4$, is that the load

vector from the previous time step is not required. This vector is available, but it is computed for a different mesh and its use will bring about complications.

The time derivative in Eq. (6), for node j, is discretized as $\mathrm{D}T/\mathrm{D}t \approx (T_j^i - T_j^{i-1})/\Delta t$, where T_j^i and T_j^{i-1} are the computed nodal values of the temperature at times i and $i-1$, respectively. The position of node j changes from time $i-1$ to time i due to the mesh movement, i.e. the temperature at the node is function of its spatial position, $\mathbf{x}$, as well as time, t. This is exactly what is implied by the total derivative and its computation comes naturally in the presented FEM discretization.

2.2. Moving mesh equations

A graphical interpretation of the adaptive mesh generation is shown for the one dimensional case by the mapping in Fig. 1. A uniform computational mesh is defined along ζ. The real physical mesh is to be generated along s. Let at s_m be the location of the phase change isotherm at a given time. A refined mesh is required towards point s_m. If a function $\zeta(s)$ is constructed such that it has a high gradient in the vicinity of s_m the mapping represented by the dotted lines will give the required mesh refinement.

The monitor function G that governs the mesh refinement is defined as:

$$G(s) = C\frac{\mathrm{d}\zeta}{\mathrm{d}s} \tag{11}$$

The construction of $\zeta(s)$ is achieved by the principal of equidistribution (i.e. the areas below $G(s)$ between consecutive mesh points to be equal) where $G(s)$ is a known function. Eq. (11) can be transformed to a boundary value problem by differentiation:

$$\frac{\mathrm{d}}{\mathrm{d}s}\left(G^{-1}\frac{\mathrm{d}\zeta}{\mathrm{d}s}\right) = 0 \tag{12}$$

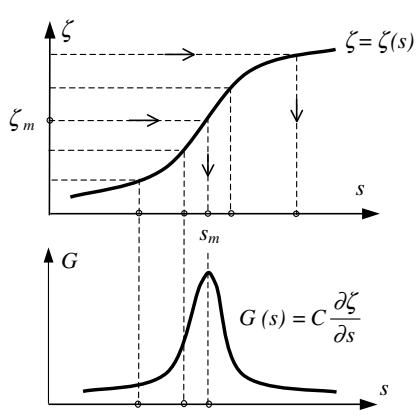

Fig. 1. Mapping from a uniform computational mesh ζ to a physical mesh s via a monitor function $G(s)$. Mesh refinement at point s_m.

In 2D the mapping is defined by minimization a functional of the form, (Cao et al., 1999):

$$\Phi(\xi,\eta) = \int_\Omega (\nabla\xi^\mathrm{T}\mathbf{G}^{-1}\nabla\xi + \nabla\eta^\mathrm{T}\mathbf{G}^{-1}\nabla\eta)\,\mathrm{d}x\,\mathrm{d}y \tag{13}$$

The Euler–Lagrange equations characterizing the extremum of Eq. (13) take the form:

$$\begin{aligned}\nabla\cdot(\mathbf{G}^{-1}\nabla\xi) &= 0\\ \nabla\cdot(\mathbf{G}^{-1}\nabla\eta) &= 0\end{aligned} \tag{14}$$

where ξ, η are coordinates in the computational 2D domain and $\mathbf{G}$ is a matrix of monitor functions:

$$\mathbf{G} = \begin{bmatrix} G_x(x,y) & 0 \\ 0 & G_y(x,y)\end{bmatrix} \tag{15}$$

To have an explicit definition of the physical coordinates Eqs. (12) and (14) have to be written in terms of $\partial s/\partial\zeta$ and $\partial\mathbf{x}/\partial\xi$ and a pseudo transient formulation is introduced to smooth out the evolution of the mesh (Beckett et al., 2001; Cao et al., 1999; Huang, 1999). A diagonal monitor function allows to decoupled the 2D equations.

$$\frac{\partial s}{\partial\tilde{t}} = \frac{1}{P_s}\left[A_s\frac{\partial^2 s}{\partial\zeta^2} + D_s\frac{\partial s}{\partial\zeta}\right] \tag{16}$$

$$\frac{\partial x}{\partial\tilde{t}} = \frac{1}{P}\left[A\frac{\partial^2 x}{\partial\xi^2} + B\frac{\partial^2 x}{\partial\xi\partial\eta} + C\frac{\partial^2 x}{\partial\eta^2} + D\frac{\partial x}{\partial\xi} + E\frac{\partial x}{\partial\eta}\right] \tag{17a}$$

$$\frac{\partial y}{\partial\tilde{t}} = \frac{1}{P}\left[A\frac{\partial^2 y}{\partial\xi^2} + B\frac{\partial^2 y}{\partial\xi\partial\eta} + C\frac{\partial^2 y}{\partial\eta^2} + D\frac{\partial y}{\partial\xi} + E\frac{\partial y}{\partial\eta}\right] \tag{17b}$$

where $A, B, \ldots, E$ are non-linear functions of the physical coordinates, P and P_s are normalizing, scaling coefficients, which are evaluated using the last known physical coordinates (see Appendix A). The steady state solution is required (i.e. $\partial s/\partial\tilde{t} = 0$, etc.) and the transient formulation ($\tilde{t}$ is a fictitious time) is used only to indicate a solution procedure that would be similar to the one used to solve the transient differential equations of the physical problem. Eq. (16) is to be solved on each continuous boundary edge whose two end points are fixed and do not move. The computed nodal coordinates on the boundary edges are to be used as Dirichlet boundary conditions for Eqs. (17).

The definition of the monitor functions in Eq. (15) is based on the work of Beckett et al. (2001):

$$\begin{aligned} G_x &= \left[1 + \sum_{i=1}^{N_X}\frac{\mu_i}{\sqrt{\mu_i^2|\mathbf{x}-\mathbf{x}_{m,i}|^2+1}}\right]\mu_L(T)\\ G_y &= \left[1 + \sum_{i=1}^{N_Y}\frac{\mu_i}{\sqrt{\mu_i^2|\mathbf{x}-\mathbf{x}_{m,i}|^2+1}}\right]\mu_L(T)\end{aligned} \tag{18}$$

The term $|\mathbf{x} - \mathbf{x}_{m,i}|$ is the distance of a point $\mathbf{x} = (x, y)$ to a curve i, which is defined discretely by the set of points $\mathbf{x}_{m,i} = (x_{m,i}, y_{m,i})$, toward which mesh refinement is required. The total number of such curves is N_x and N_y for mesh movement in the x and y directions, respectively. Coefficients μ_i governs the mesh refinement towards curve i which is either the phase change front or the fixed boundaries where thermal and velocity layers are to be resolved. These boundaries are different for the x and y mesh movement equations. For example, in the melting problem described later in Fig. 2, the mesh is refined only towards the left boundary in the x equation (17a). There is no need to refine towards the right boundary because the material near it is expected to be in solid state throughout the whole solution. Refinement towards the top and bottom boundaries is used in the y equation (17b). Alternatively, instead of including the boundaries into the monitor function, the computational mesh can be refined at the corresponding boundaries. This, however, will require the actual generation of a computational mesh. Coefficient $\mu_L(T)$, allows the mesh to be refined in the liquid region at the expense of the solid one: $\mu_L = 1$ if $T < T_m$ and $\mu_L > 1$ otherwise.

2.2.1. FEM approximation

Galerkin's discretization of Eqs. (17), on an element level, results in:

$$\int\int_\Omega \mathbf{N}^T\mathbf{N}\,d\Omega\frac{\partial \mathbf{x}}{\partial t} - \int\int_\Omega \mathbf{N}^T\frac{1}{P}\left[A\frac{\partial^2\mathbf{N}}{\partial\xi^2} + C\frac{\partial^2\mathbf{N}}{\partial\eta^2} + B\frac{\partial^2\mathbf{N}}{\partial\xi\partial\eta} + D\frac{\partial\mathbf{N}}{\partial\xi} + E\frac{\partial\mathbf{N}}{\partial\eta}\right]d\Omega\,\mathbf{x} = 0 \tag{19}$$

Note: The computational coordinates ξ, η should not be confused with the local element coordinates. However, when the computational mesh is uniform, i.e. there are no mesh refinements towards the fixed boundaries, the computational domain may be chosen in such a way, so that the computational element to be identical to the isoparametric, non-dimensional, finite element. In this case there is no need to construct a computational mesh.

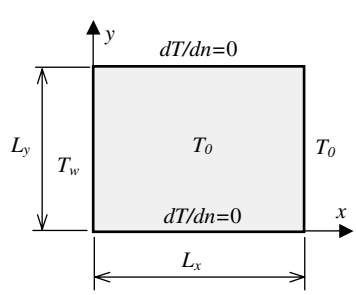

Fig. 2. Layout of test problems. Melting problems: $L_x = L_y = 1$; $T_w = 1$; $T_0 = 0$; $T_m = 0$. Freezing problem: $L_x = 0.3$ m; $L_y = 0.15$ m; $T_w = -10$ °C; $T_0 = 10.2$ °C; $T_m = 0$ °C.

Integrating by parts and ignoring the boundary line integrals, because Dirichlet boundary conditions will be used on all boundaries, results in:

$$-\int\int_\Omega \mathbf{N}^T\frac{A}{P}\frac{\partial^2\mathbf{N}}{\partial\xi^2}\,d\Omega = \int\int_\Omega \frac{\partial(\mathbf{N}^T A/P)}{\partial\xi}\frac{\partial\mathbf{N}}{\partial\xi}\,d\Omega = \int\int_\Omega \mathbf{N}^T\frac{\partial(A/P)}{\partial\xi}\frac{\partial\mathbf{N}}{\partial\xi}\,d\Omega + \int\int_\Omega \frac{\partial\mathbf{N}^T}{\partial\xi}\frac{A}{P}\frac{\partial\mathbf{N}}{\partial\xi}\,d\Omega \tag{20}$$

$$-\int\int_\Omega \mathbf{N}^T\frac{C}{P}\frac{\partial^2\mathbf{N}}{\partial\eta^2}\,d\Omega = \int\int_\Omega \frac{\partial(\mathbf{N}^T C/P)}{\partial\eta}\frac{\partial\mathbf{N}}{\partial\eta}\,d\Omega = \int\int_\Omega \mathbf{N}^T\frac{\partial(C/P)}{\partial\eta}\frac{\partial\mathbf{N}}{\partial\eta}\,d\Omega + \int\int_\Omega \frac{\partial\mathbf{N}^T}{\partial\eta}\frac{C}{P}\frac{\partial\mathbf{N}}{\partial\eta}\,d\Omega \tag{21}$$

$$-\int\int_\Omega \mathbf{N}^T\frac{B}{P}\frac{\partial^2\mathbf{N}}{\partial\xi\partial\eta}\,d\Omega = \frac{1}{2}\left[\int\int_\Omega \frac{\partial(\mathbf{N}^T B/P)}{\partial\xi}\frac{\partial\mathbf{N}}{\partial\eta}\,d\Omega + \int\int_\Omega \frac{\partial(\mathbf{N}^T B/P)}{\partial\eta}\frac{\partial\mathbf{N}}{\partial\xi}\,d\Omega\right] \tag{22}$$

The averaging procedure is used in Eq. (22) to eliminate any bias in the integration by parts. The remaining terms need not be modified. After the finite element spatial discretization, the resulting system of ordinary differential equations takes the form:

$$\mathbf{M}\frac{d\mathbf{x}}{d\tilde{t}} + (\mathbf{A} + \mathbf{B} + \mathbf{C} + \mathbf{D} + \mathbf{E})\mathbf{x} = 0, \tag{23}$$

where the matrices $\mathbf{M}, \mathbf{A}, \ldots, \mathbf{E}$, are given in Appendix A. To solve (23) the system is first linearised by evaluating the matrices $\mathbf{A}, \ldots, \mathbf{E}$ using the mesh and the solution at the current time step. The resulting linear set of equations is solved using an ILU-preconditioned BICGstab routine. As the current mesh is usually a good initial guess only a finite number (usually around 10) BICGstab iterations are performed.

The reason for using only Dirichlet boundary conditions (which can be determined by solving the 1D moving mesh equations on all boundaries) is that the Neumann boundary conditions corresponding to the boundary integrals are not known. In the finite element approximation it is possible to assume symmetry boundary conditions along each boundary curve. In this case the 1D moving mesh equations need not be solved. However, in some cases, Eq. (23) may become ill-conditioned and the moving mesh to be unstable. On the other hand the 1D mesh movement on a boundary edge is not identical to the mesh movement that would be calculated for this edge by the 2D formulation. The differences die away quickly, but it is possible to present some numerical problems, if a proper temporal smoothing (i.e. suitable fictitious time step $\Delta\tilde{t}$) is not used.

2.3. Navier–Stokes equations

Assuming density to be constant except in the buoyancy term (Boussinesq approximation) and that the only body force is due to the gravity acceleration in the y direction, the Navier–Stokes equations for a stationary mesh are:

$$\frac{\partial u}{\partial t} + \mathbf{u}\cdot\nabla u - \nabla\cdot\left(\frac{\mu}{\rho_0}\nabla u\right) = -\frac{1}{\rho_0}\frac{\partial p}{\partial x} \tag{24}$$

$$\frac{\partial v}{\partial t} + \mathbf{u}\cdot\nabla v - \nabla\cdot\left(\frac{\mu}{\rho_0}\nabla v\right) = -\frac{1}{\rho_0}\left(\frac{\partial p}{\partial y} + \rho g\right) \tag{25}$$

$$\frac{\partial u}{\partial x} + \frac{\partial v}{\partial y} = 0 \tag{26}$$

The incompressibility condition, Eq. (26), may be relaxed by using a penalty formulation for the pressure (Heinrich and Pepper, 1996):

$$p = p_s - \lambda\left(\frac{\partial u}{\partial x} + \frac{\partial v}{\partial y}\right) \tag{27}$$

The derivatives of the hydrostatic pressure p_s are:

$$\frac{\partial p_s}{\partial x} = 0; \quad \frac{\partial p_s}{\partial y} = -\rho_0 g \tag{28}$$

Substituting Eqs. (27) and (28) into Eqs. (24) and (25), gives:

$$\begin{aligned}
&\frac{\partial u}{\partial t} + \mathbf{u}\cdot\nabla u - \nabla^{\mathrm{T}}\left(\frac{\mu}{\rho_0}\nabla u\right) - \frac{\lambda}{\rho_0}\frac{\partial}{\partial x}\left(\frac{\partial u}{\partial x} + \frac{\partial v}{\partial y}\right) = 0\\
&\frac{\partial v}{\partial t} + \mathbf{u}\cdot\nabla v - \nabla^{\mathrm{T}}\left(\frac{\mu}{\rho_0}\nabla v\right)\\
&\quad - \frac{\lambda}{\rho_0}\frac{\partial}{\partial y}\left(\frac{\partial u}{\partial x} + \frac{\partial v}{\partial y}\right) = \frac{(\rho_0 - \rho)g}{\rho_0}
\end{aligned} \tag{29}$$

Taking into account the mesh movement in a similar way as in the energy equation, the final form of the equations to be solved by FEM is

$$\begin{aligned}
&\frac{\mathrm{D}u}{\mathrm{D}t} + \mathbf{u}\cdot\nabla u - \frac{\mathrm{d}\mathbf{x}}{\mathrm{d}t}\cdot\nabla u - \nabla^{\mathrm{T}}\left(\frac{\mu}{\rho_0}\nabla u\right)\\
&\quad - \frac{\lambda}{\rho_0}\frac{\partial}{\partial x}\left(\frac{\partial u}{\partial x} + \frac{\partial v}{\partial y}\right) = 0\\
&\frac{\mathrm{D}v}{\mathrm{D}t} + \mathbf{u}\cdot\nabla v - \frac{\mathrm{d}\mathbf{x}}{\mathrm{d}t}\cdot\nabla v - \nabla^{\mathrm{T}}\left(\frac{\mu}{\rho_0}\nabla v\right)\\
&\quad - \frac{\lambda}{\rho_0}\frac{\partial}{\partial y}\left(\frac{\partial u}{\partial x} + \frac{\partial v}{\partial y}\right) = \frac{(\rho_0 - \rho)g}{\rho_0}
\end{aligned} \tag{30}$$

The finite element approximation is given in Appendix B.

3. Numerical examples

A schematic presentation of the test problems is given in Fig. 2.

3.1. Melting problems

The melting problems solved are those considered by Gobin and Le Quéré (2000). They compared the numerical solutions presented by 13 contributors using different methods and software. They make no comparison with experimental results because, to the best of their knowledge, reliable results are not available. Here we solve three of the four cases presented by Gobin and Le Quéré (2000), keeping their original numbering. The case that is not solved has a very low *Ra* number and melting is dominated by conduction. It is very close to the Stefan problem, in which convection is neglected. The latter has been solved for all considered test cases as a first check for the moving mesh formulation.

The transition from the dimensionless numbers to the material data used in the presented equations is as

Table 1
Melting problems: material data (in terms of dimensionless numbers)

	Pr	*Ste*	*Ra*	τ
Case 2	0.02	0.01	2.5×10^5	0.04
Case 3	50	0.1	1.0×10^7	0.01
Case 4	50	0.1	1.0×10^8	0.01

Table 2
Melting without convection. Comparison of FEM moving mesh with analytical results

Mesh	μ_1	Time steps	Error % at τ			Max. abs. error%		
			Case 2	Case 3	Case 4	Case 2	Case 3	Case 4
15×1	200	300	0.065	−0.076	−0.076	0.896	0.987	0.987
		600	−0.224	−0.055	−0.055	0.987	0.641	0.641
	600	300	0.206	−0.037	−0.037	0.301	0.288	0.288
		600	0.205	0.026	0.026	0.301	0.388	0.388
45×1	200	300	0.082	0.076	0.076	0.598	0.383	0.383
		600	−0.016	0.007	0.007	0.515	0.313	0.313
	600	300	−0.267	0.050	0.050	0.622	0.254	0.254
		600	0.029	0.005	0.005	0.331	0.195	0.195

follow: $\rho_0 = \sqrt{Ra/Pr}$ [kg/m^3]; $c = Pr$ [J/kg °C]; $h = Pr/Ste$ [J/kg]; $t = \frac{\sqrt{Ra \times Pr}}{Ste}\tau$ [s]; $\mu = 1$ [kg/m s]; $\beta = 1$ [1/°C]; $k = 1$[J/(m s °C)]; $g = 1$ [m/s^2]; $T_w = 1$ °C; $T_0 = 0$ °C; $L = 1$ [m]; $\rho = \rho_0(1 - \beta(T_w - T))$ [kg/m^3]. These numbers are given in Table 1. The time τ is the time when results are compared.

3.1.1. Melting without convection

The test problems are first solved neglecting convection. The results are compared with the one-dimensional analytical solution of the Stefan problem, used also by Mackenzie and Robertson (2000). The finite element mesh is a single row of rectangular elements in the x-direction. The error in the position of the melting front at time τ and the maximum error from all time steps are presented in Table 2.

$$\text{Error}\% = \frac{x_{\text{FEM}} - x_{\text{Analytical}}}{L_x} 100\% \tag{31}$$

To smooth out the initial temperature discontinuity between the hot wall and the interior, smaller time steps are used in the beginning of the analysis. The first 100 time steps increase in a geometric progression with a factor 1.07. The remaining time steps are equal to the 100th one. The phase change temperature interval (PCTI) is $\varepsilon = \varepsilon_1 + \varepsilon_2$ with $\varepsilon_1 = \varepsilon_2 = 0.01$. The initial temperature in the solid and the boundary condition on the right wall are dropped down by $1.1\varepsilon_1$ in order to accommodate the whole PCTI.

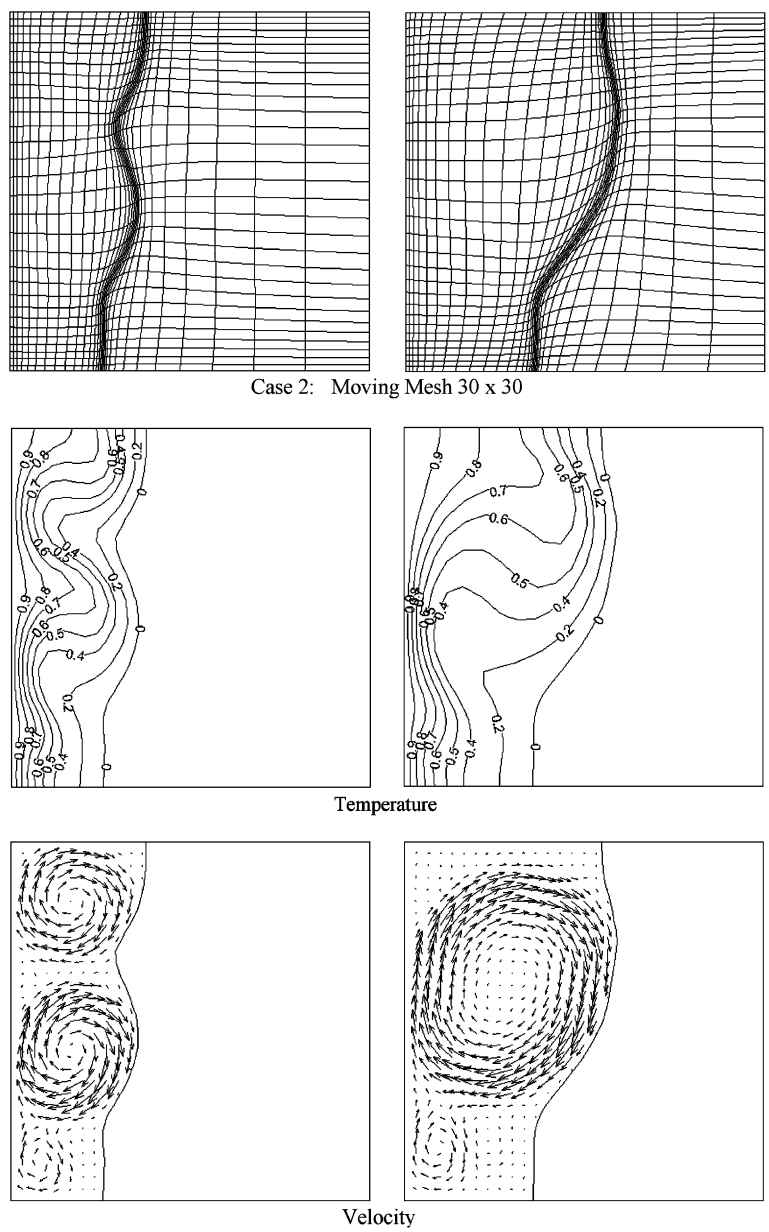

Fig. 3. Case 2: Mesh, temperature and velocity at time $\tau = 0.04$ (left) and $\tau = 0.08$ (right).

The FEM moving mesh results are in very good agreement with the analytical solution and do not depend on the computational parameters when they are varied within reasonable bounds. The latter are determined by two combinations of the parameters:

(i) The number of elements, the level of the mesh refinement governed by μ_1, and the magnitude of ε should ensure that there are at least 3–4 elements across the width of the PCTI. Thus the numerical integration of the large discontinuity in the apparent heat capacity can be done sufficiently accurately. The error occurs in the elements through which the isotherms $(T_m - \varepsilon_1)$ or $(T_m + \varepsilon_2)$ pass. Increasing the number of the Gauss integration points for these elements does not help much because the convergence rate is very low.

(ii) The magnitudes of the time step and ε should ensure that the area under the PCTI progresses by overlapping its previous position and does not leave any volumes that change phase without being exposed to the effect of the latent, i.e. being in a mushy state.

The PCTI is the most important parameter. If it has small values it is more likely not to meet the above requirements and the solution would be more inaccurate. However, using large values for the PCTI modifies

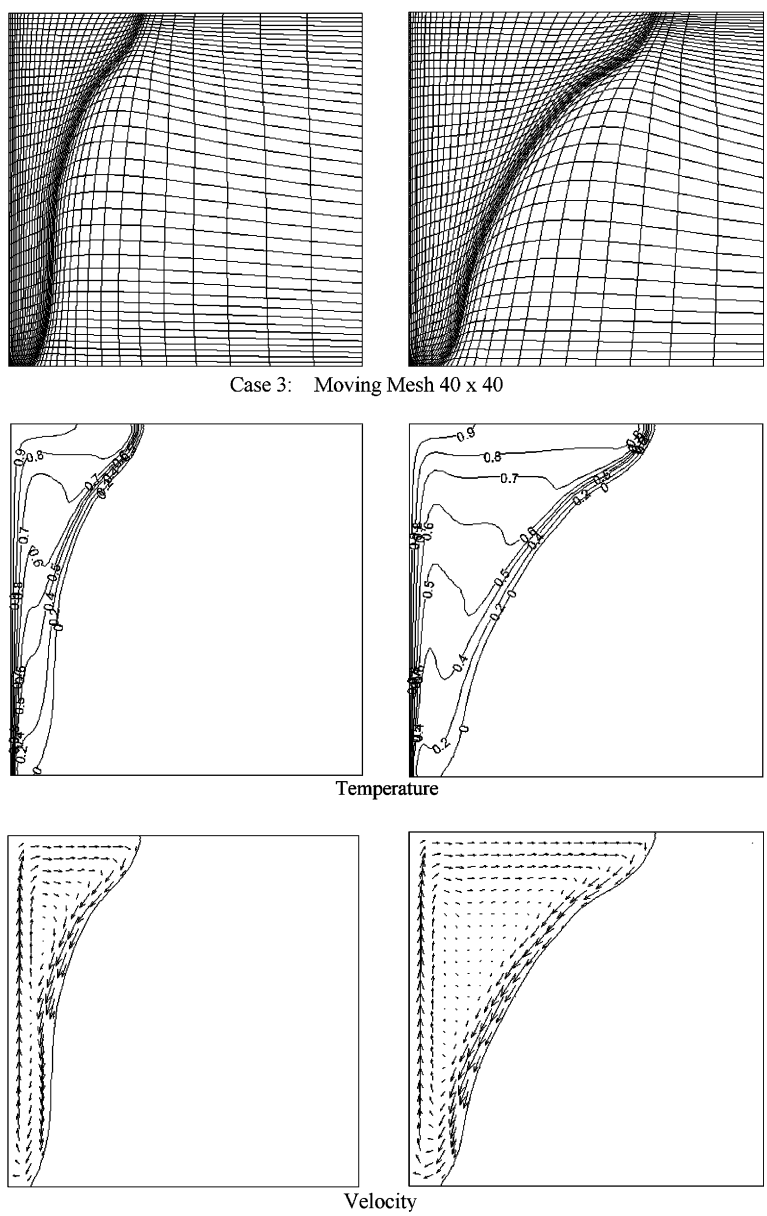

Fig. 4. Case 3: Mesh, temperature and velocity at time $\tau = 0.01$ (left) and $\tau = 0.02$ (right).

the actual physical problem, which can become unacceptable, especially, when the phase change is isothermal. The need for a proper choice of the PCTI may be avoided if the apparent heat capacity is defined by means of the enthalpy H

$$\rho c = \frac{\mathrm{d}H}{\mathrm{d}T} \approx \frac{\mathrm{d}H/\mathrm{d}x}{\mathrm{d}T/\mathrm{d}x} \tag{32}$$

where the approximation is written for the 1D formulation of the problem. Having to approximate $\mathrm{d}H/\mathrm{d}x$ and $\mathrm{d}T/\mathrm{d}x$ discretely means that the phase change cannot be omitted. Furthermore, in a finite element context this approach takes into account the influence of all points in the element and this has a smoothing effect which again can be reduced if the elements close to the melting isotherm are small.

However, a refined mesh at the phase change front will require small time steps to avoid the large jumps of the mushy phase, as discussed in (ii). It is possible to have good engineering solutions (error < 5%) of 1D test problems with a suitable combination of large time steps and small element size in which a large volume (more than 50%) undergoes phase transition without passing through the mushy state. This accuracy can be achieved because the energy error accumulated in this volume can be partially cancelled out by the energy error in the 'mushy' volume, which has been in a mushy state for longer than necessary.

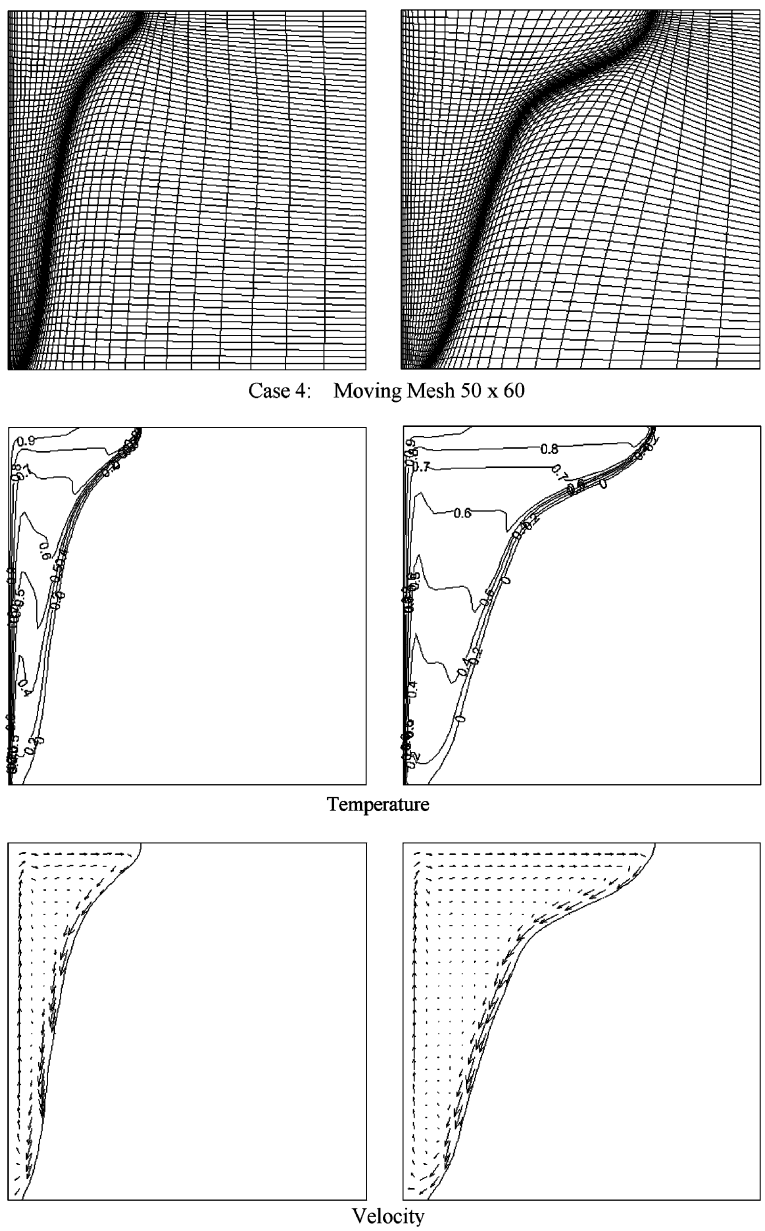

Fig. 5. Case 4: Mesh, temperature and velocity at time $\tau = 0.005$ (left) and $\tau = 0.01$ (right).

In the case of general 2D phase change problems various spatial approximations of Eq. (32) have been proposed (Dalhuijsen and Segal, 1981). Our numerical studies have shown that in these cases it is more difficult to get the above error canceling effect and that, on average, better accuracy is achieved when the apparent heat capacity is given in terms of the phase change temperature interval, Eq. (5).

3.1.2. Melting with natural convection

The moving mesh, temperature and velocity at two time steps for Cases 2–4 are shown in Figs. 3–5, respectively. In Case 2 the velocity field is dominated by the presence of recirculation rolls. There are more rolls at the early stages of the melting process when the aspect ratio y/x of the liquid region is bigger. As the melting front propagates towards the interior the rolls merge and decrease in number. These rolls cause the wavy shape of the melting front and they are numerically predicted by most analyses presented by Gobin and Le Quéré (2000). It has been established by a careful mesh refinement study (Hannoun et al., 2003) that this velocity pattern is the correct solution of the mathematical problem, although the existence of such rolls has not still been reported experimentally. In Case 3 recirculation rolls are observed at the very early stages of the melting and they soon collapse into one circulation. For Case 4, with the meshes and time steps used, recirculation rolls are not observed. These two cases are characterized by high velocities (strong convective contribution in the transport equation) and very thin thermal boundary layers. Computationally they are more demanding (finer meshes and smaller time steps) and more difficult to solve than Case 2.

In Fig. 6 the computed phase change front using the moving mesh technique (solid lines) and the range of variation of the numerical results (dotted lines) given by Gobin and Le Quéré (2000) are plotted. They define a range of best solutions, which is presented in Fig. 6 by the dashed lines. For the three cases the moving mesh results lie within the range of the best solutions. Only two results show such accuracy—by Le Quéré, results No 10, and by Wintruff, results No 13. The former uses a one-domain, 'enthalpy' formulation and the latter uses a front tracking technique. Two more results using the one-domain formulation are within the best solutions for Case 2 and Case 3, but have not solved Case 4. The meshes $NX \times NY$ and the time steps used are presented in Table 3.

The additional user definable data used in the FEM analyses are give in Table 4. The initial and the right wall boundary temperature T_0 is lowered by $1.5\varepsilon_1$ in order to accommodate the phase change interval. Numerical studies have shown that better accuracy is achieved when the phase change interval lies entirely within the temperature of the phase that is going to change phase, i.e. into

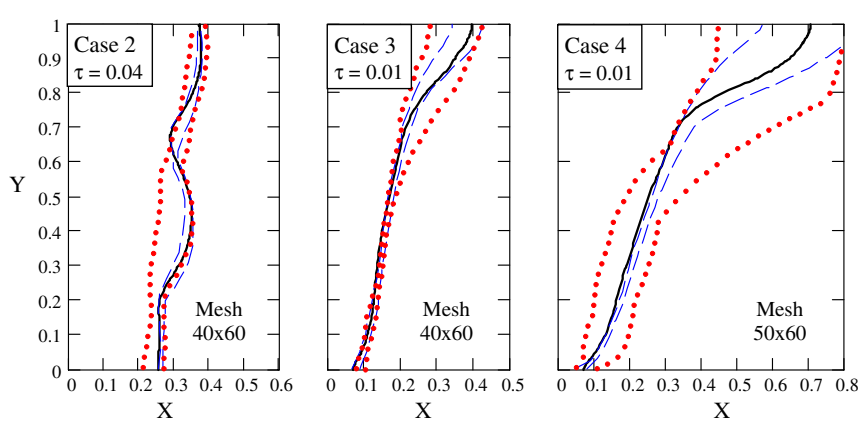

Fig. 6. Position of the phase change front at time τ. Solid line—FEM moving mesh solution. Area between dotted lines—range of all numerical solutions by Gobin and Le Quéré (2000); Area between dashed lines—range of best numerical solutions by Gobin and Le Quéré (2000).

Table 3
Mesh and time steps used in FEM moving mesh analyses and in the 'best' solutions given by Gobin and Le Quéré (2000)

	Moving mesh		Le Quéré (No. 10)		Couturier-Sadat (No. 6)		Médale (No. 11)	
	Mesh	$\Delta\tau$	Mesh	$\Delta\tau$	Mesh	$\Delta\tau$	Mesh	$\Delta\tau$
Case 2	30×30	2.5×10^{-5}	128×192	2×10^{-7}	202×202	1×10^{-5}	100×50	1×10^{-4}
Case 3	40×40	6.6×10^{-6}	No data		122×122	2×10^{-6}	200×100	1×10^{-5}
Case 4	50×60	2.5×10^{-6}	192×192	1×10^{-7}	Not solved		Not solved	

Table 4
Computational parameters used in the FEM moving mesh analyses

	ε_1	ε_2	μ_1	μ_2	μ_L
Case 2	0.02	0.0	300	50	1.2
Case 3	0.02	0.0	100	50	2.0
Case 4	0.05	0.0	200	100	1.5

the solid for melting problems and into the liquid for solidification problems. The values of μ_1 may be interchanged without affecting the accuracy, which is later shown in the sensitivity study. Case 4 has narrower thermal boundary layers and thus needs more mesh refinement towards the boundaries, i.e. higher values for μ_2.

In Fig. 7 the evolution of the averaged Nusselt number on the hot wall is presented. The numerical results presented by Gobin and Le Quéré (2000) show again a large scatter. The moving mesh results are close to the empirical correlation for Case 3 and Case 4. For Case 2 they are very close to Le Quéré's results, which form the upper bound of the numerical solutions.

In Figs. 8 and 9 the sensitivity of the position of the phase change front on the variation of some user definable parameters can be observed for Case 2 and Case 3, respectively. Similar low sensitivity behaviour is computed for Case 4 and that is why these results are not presented. The time for the numerical simulation τ is given in Table 1 and the computational parameters that are not varied explicitly are those given in Table 4. To extend the sensitivity study different number of times steps, N_τ, are used as follow—Case 2: $N_\tau = 1000$ for problems in Fig. 8A, $N_\tau = 300$ for Fig. 8B and C; Case 3: $N_\tau = 1500$ for Fig. 9A and C, $N_\tau = 700$ for Fig. 9B.

It can be seen that the parameters can be varied in a wide range without having a considerable effect on the position of the phase change front. The interaction between the parameters and the reasonable bounds of their variation are the same as discussed previously in

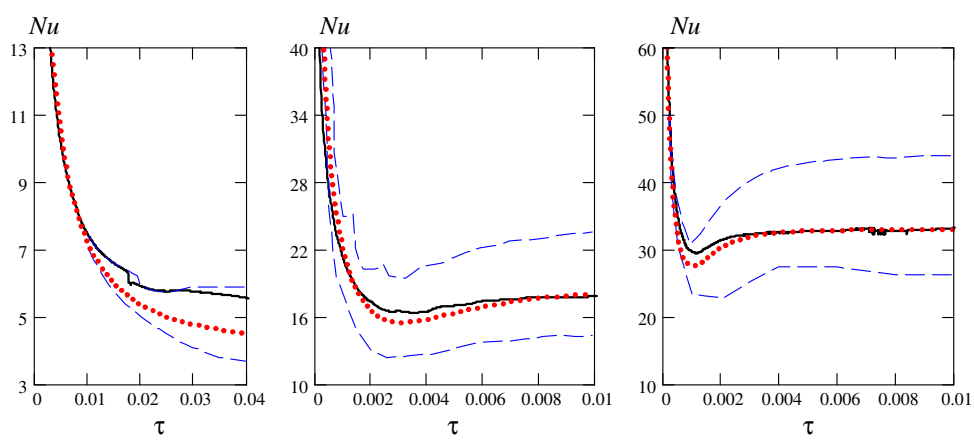

Fig. 7. Evolution of the averaged Nusselt number on the hot wall. Solid line—FEM results; Dashed lines—range of variation of numerical results by Gobin and Le Quéré (2000). Dotted line—target result (empirical correlation) by Gobin and Le Quéré (2000).

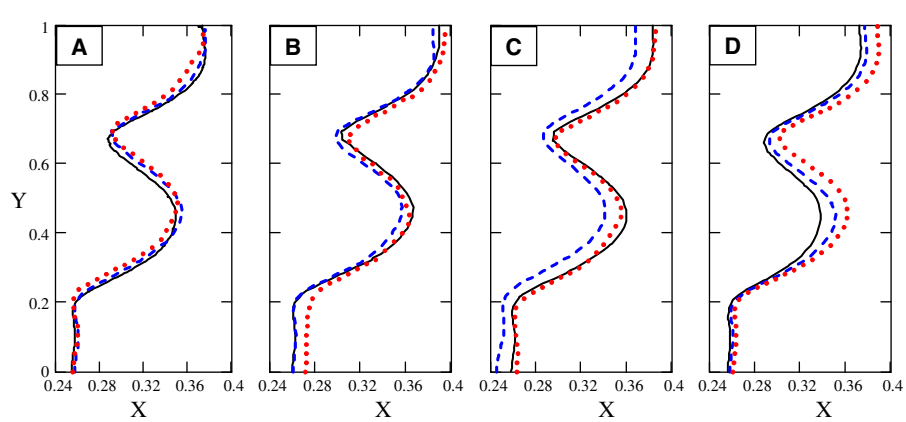

Fig. 8. Case 2: Position of the phase change front–sensitivity study. (A) '1': mesh 40×60, '2': mesh 30×30, '3': mesh 20×25. (B) '1': $\mu_1 = 500$, '2': $\mu_1 = 100$, '3': $\mu_1 = 20$. (C) '1': $\varepsilon_1 = 0.02$, '2': $\varepsilon_1 = 0.10$, '3': $\varepsilon_1 = 0.01$. (D) '1': $N_\tau = 1200$, '2': $N_\tau = 600$, '3': $N_\tau = 200$. Graphs: '1': solid lines, '2': dashed lines, '3': dotted lines.

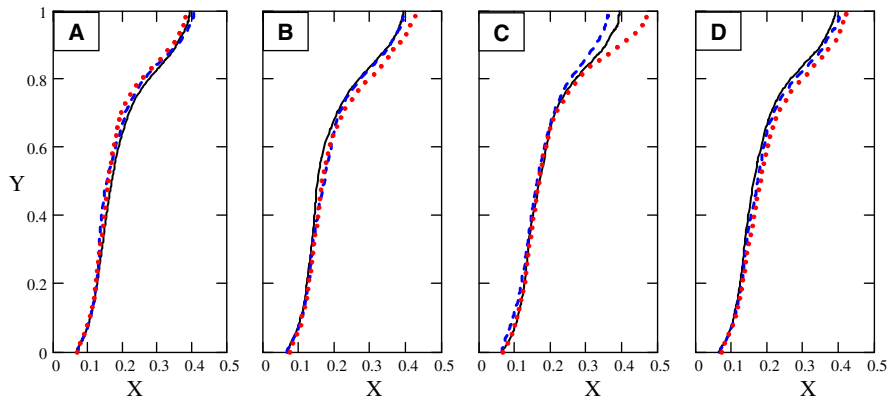

Fig. 9. Case 3: Position of the phase change front–sensitivity study. (A) '1': mesh 70 × 110, '2': mesh 40 × 40, '3'—mesh 30 × 60. (B) '1': $\mu_1 = 200$, '2': $\mu_1 = 100$, '3': $\mu_1 = 50$. (C) '1': $\varepsilon_1 = 0.02$, '2': $\varepsilon_1 = 0.10$, '3': $\varepsilon_1 = 0.01$. (D) '1': $N_\tau = 1000$, '2': $N_\tau = 500$, '3': $N_\tau = 250$. Graphs: '1': solid lines, '2': dashed lines, '3': dotted lines.

(i) and (ii). The presence of fluid flow imposes two additional limitations. First, there should be enough elements in the fluid phase to model correctly the fluid flow. For the same reason the mesh should not be over refined at the phase change interval. Second, the time step should be small enough to allow correct modeling of the fluid flow. When a small number of time steps are used the velocity becomes more unstable between time steps (e.g. it has a wavy pattern along the top boundary). This velocity instability seems to be the primary reason for the variation in the position of the phase change front in Fig. 8D. When the fluid flow is ignored (see results in Table 2, computed with a small number of time steps) the errors are very small.

Increasing the PCTI in Fig. 8C from $\varepsilon_1 = 0.01$ to $\varepsilon_1 = 0.02$ has almost no influence on the predicted position of the phase change front. A decrease of ε_1 (not shown on the graph, but observed during the numerical sensitivity studies) causes the front to propagate faster because the number of elements in the mushy region is reduced and the latent heat is not accounted for properly. A large ε_1 reduces the accuracy, too, because the physical problem has been changed ($\varepsilon_1 = 0.1$ is 10% of the temperature range in the problem).

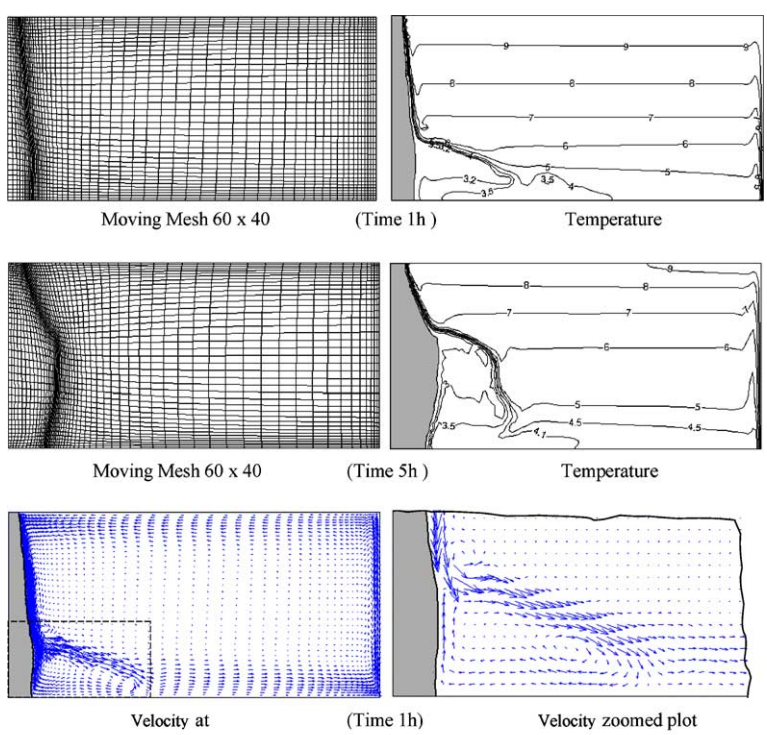

Fig. 10. Water freezing: Mesh and temperature at time $t = 1$ h and 5 h and velocity at $t = 1$ h.

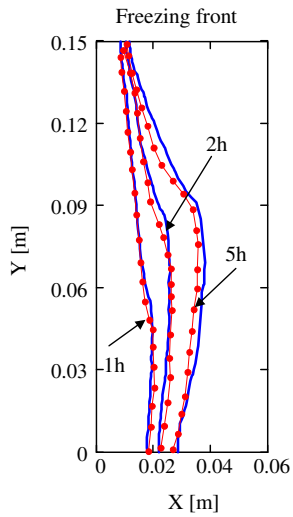

Fig. 11. Water freezing: Position of the phase change front at times $t = 1$ h, 2 h and 5 h. Solid line: FEM results (moving mesh 60×40). Dotted line (●): Experimental data by Braga and Viskanta (1992).

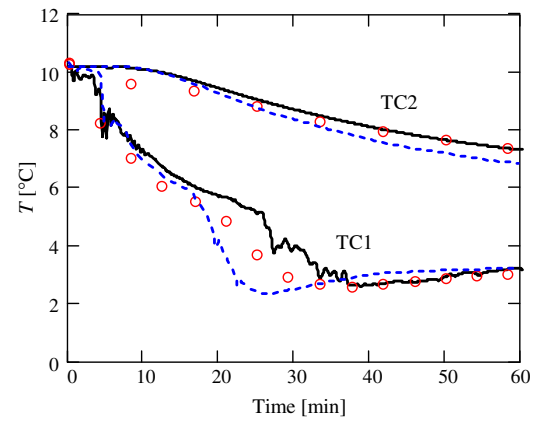

Fig. 12. Water freezing. Comparison with published results. Temperature at thermocouples TC1 and TC2. Solid line—FEM results (moving mesh 60×40); Dots 'o'—Experimental data by Braga and Viskanta (1992); Dashed line—Numerical results by Scanlon and Stickland (2004), FLUENT analysis (finite volume method) with a fixed mesh 300×200 elements.

3.2. Freezing problem

Freezing of water on the vertical wall of a rectangular cavity is studied. The outline of the problem is presented in Fig. 2. It has been studied experimentally by Braga and Viskanta (1992) and numerically by Scanlon and Stickland (2004). The water density as a function of T [°C] is approximated as (Scanlon and Stickland, 2004):

$$\rho(T) = 999.972(1 - 9.2793 \times 10^{-6}|T - 4.0293|^{1.894816}) \ [\mathrm{kg/m^3}] \tag{33}$$

The moving mesh of 60 by 40 elements (along x and y, respectively), the temperature isotherms at times $t = 1$ h and $t = 5$ h, and the velocity at $t = 1$ h are shown in Fig. 10. The density inversion at 4.0293 °C is responsible for the flow structure with a big anti-clockwise circulation where $T > 4.0293$ °C and a small clockwise one at the bottom left where $T < 4.0293$ °C. The same pattern has been observed experimentally by Braga and Viskanta (1992) and numerically by Scanlon and Stickland (2004).

The position of the phase change front at several times is shown in Fig. 11. At time $t = 1$ h and $t = 2$ h there is a very good agreement with the experimental results by Braga and Viskanta (1992). At $t = 5$ h the agreement is generally good with the exception that the computed ice thickness is larger. It is possible that the error is due to computed lower velocities near the freezing boundary (in Braga and Viskanta (1992) there is no data of the magnitude of the experimental velocities).

The temperature histories at the location of two thermocouples, TC1 ($x = 0.05$ m, $y = 0.02$ m) and TC2 ($x = 0.15$ m, $y = 0.075$ m) are shown in Fig. 12. There is good agreement with the experimental results by Braga and Viskanta (1992), and the numerical results by Scanlon and Stickland (2004). It should be noted that the latter are achieved by finite volume method (Fluent software) using a mesh of 300×200 elements which was obtained via a grid refinement study.

In Fig. 13 the results of a sensitivity study are shown. The error of the position of the phase change front is computed by comparing the FEM and experimental x-coordinates of the freezing front at time $t = 60$ min, at 50 pre-defined, uniformly distributed locations along y.

$$\mathrm{Error} = \left[\sum_{i=1}^{50}(x_{\mathrm{FEM}} - x_{\mathrm{exp}})^2\right]^{\frac{1}{2}} \left[\sum_{i=1}^{50} x_{\mathrm{exp}}\right]^{-1} \times 100\% \tag{34}$$

It can be seen that the accuracy decreases when $\mu < 200$ and it is almost independent on the number time steps and number of elements used. The investigation of the phase change temperature interval ε shows that it has an optimal value of about 1.5 °C and that better accuracy is achieved when $\varepsilon_1 = 0$, i.e. when ε is situated entirely into the phase that is going to change phase.

4. Conclusions

An r-adaptive moving mesh technique has been successfully applied to the solution of phase change problems with natural convection. The generation of the moving mesh requires the solution of two extra partial differential equations at each time step. The main advantage of the method is that less number of elements may be used. The accuracy is preserved because the mesh is kept sufficiently refined around the phase change at all times. The numerical experiments in this paper have been computed on rectangular domains. For more complicated non-

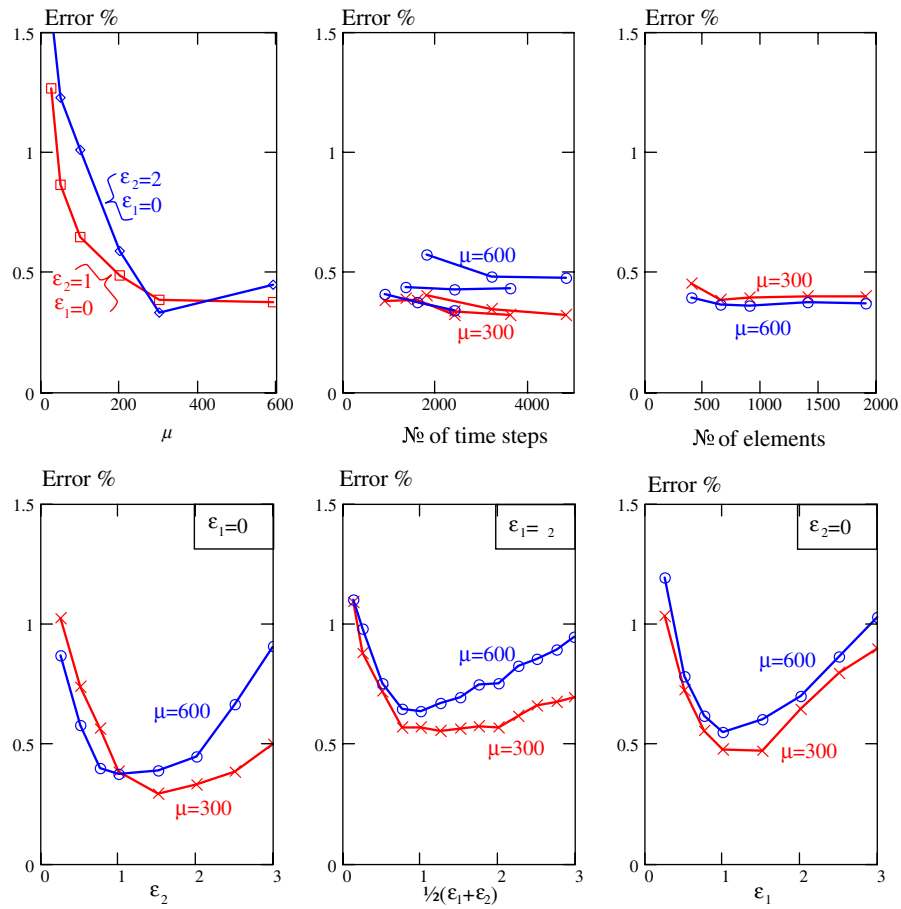

Fig. 13. Sensitivity study of the accuracy of the position of the freezing front at $t = 60$ min; ε_1 and ε_2 define the variation of the phase change interval: $T_m - \varepsilon_1 \leqslant T \leqslant T_m + \varepsilon_2$; μ is a parameter in the monitor function G, Eq. (18), defining the mesh density towards the phase change front (the bigger μ the more refined is the mesh).

convex domains the moving mesh method can be extended as shown by Cao et al. (1999), and we leave work in this direction for further investigation.

Acknowledgement

The authors would like to acknowledge the EPSRC financial support, grant No. GR/R2603/01.

Appendix A

Moving mesh equations on the boundary edges:

$$\frac{\partial s}{\partial \tilde{t}} = \frac{1}{P_s}\frac{\partial}{\partial \zeta}\left(G\frac{\partial s}{\partial \zeta}\right) = \frac{1}{P_s}\left[G\frac{\partial^2 s}{\partial \zeta^2} + \frac{\partial G}{\partial \xi}\frac{\partial s}{\partial \zeta}\right] = \frac{1}{P_s}\left[A_s\frac{\partial^2 s}{\partial \zeta^2} + D_s\frac{\partial s}{\partial \zeta}\right] \tag{A.1}$$

$$A_s = G; \quad D_s = \frac{\partial G}{\partial \xi}; \quad P_s = \sqrt{A_s^2 + D_s^2}$$

Moving mesh equations in the interior:

$$\frac{\partial \mathbf{x}}{\partial \tilde{t}} = \frac{1}{P}\left[A\frac{\partial^2 \mathbf{x}}{\partial \xi^2} + B\frac{\partial^2 \mathbf{x}}{\partial \xi \partial \eta} + C\frac{\partial^2 \mathbf{x}}{\partial \eta^2} + D\frac{\partial \mathbf{x}}{\partial \xi} + E\frac{\partial \mathbf{x}}{\partial \eta}\right] \tag{A.2}$$

Coefficients:

$$A = \frac{1}{J^2 G}\left(\frac{\partial x}{\partial \eta}\frac{\partial x}{\partial \eta} + \frac{\partial y}{\partial \eta}\frac{\partial y}{\partial \eta}\right);$$

$$C = \frac{1}{J^2 G}\left(\frac{\partial x}{\partial \xi}\frac{\partial x}{\partial \xi} + \frac{\partial y}{\partial \xi}\frac{\partial y}{\partial \xi}\right) \tag{A.3}$$

$$B = \frac{-2}{J^2 G}\left(\frac{\partial x}{\partial \xi}\frac{\partial x}{\partial \eta} + \frac{\partial y}{\partial \xi}\frac{\partial y}{\partial \eta}\right) \tag{A.4}$$

$$D = \frac{1}{J^2 G^2}\left\{\left(\frac{\partial x}{\partial \eta}\frac{\partial x}{\partial \eta} + \frac{\partial y}{\partial \eta}\frac{\partial y}{\partial \eta}\right)\frac{\partial G}{\partial \xi} - \left(\frac{\partial x}{\partial \xi}\frac{\partial x}{\partial \eta} + \frac{\partial y}{\partial \xi}\frac{\partial y}{\partial \eta}\right)\frac{\partial G}{\partial \eta}\right\} \tag{A.5}$$

$$E = \frac{1}{J^2 G^2}\left\{\left(\frac{\partial x}{\partial \xi}\frac{\partial x}{\partial \xi} + \frac{\partial y}{\partial \xi}\frac{\partial y}{\partial \xi}\right)\frac{\partial G}{\partial \eta} - \left(\frac{\partial x}{\partial \xi}\frac{\partial x}{\partial \eta} + \frac{\partial y}{\partial \xi}\frac{\partial y}{\partial \eta}\right)\frac{\partial G}{\partial \xi}\right\} \tag{A.6}$$

$$P = \sqrt{A^2 + C^2 + D^2 + E^2}; \quad J = \frac{\partial x}{\partial \xi}\frac{\partial y}{\partial \eta} - \frac{\partial x}{\partial \eta}\frac{\partial y}{\partial \xi} \tag{A.7}$$

Finite element approximation (on an element level):

$$\mathbf{M}\frac{\mathrm{d}\mathbf{x}}{\mathrm{d}t} + (\mathbf{A}+\mathbf{B}+\mathbf{C}+\mathbf{D}+\mathbf{E})\mathbf{x} = 0 \tag{A.8}$$

where

$$\mathbf{M} = \int\int_{\Omega} \mathbf{N}^{\mathrm{T}}\mathbf{N}\,\mathrm{d}\Omega \tag{A.9a}$$

$$\mathbf{A} = \int\int_{\Omega} \frac{\partial \mathbf{N}^{\mathrm{T}}}{\partial \xi}\frac{A}{P}\frac{\partial \mathbf{N}}{\partial \xi}\,\mathrm{d}\Omega \tag{A.9b}$$

$$\mathbf{B} = \frac{1}{2}\left[\int\int_{\Omega} \frac{\partial \mathbf{N}^{\mathrm{T}}}{\partial \xi}\frac{B}{P}\frac{\partial \mathbf{N}}{\partial \eta}\,\mathrm{d}\Omega + \int\int_{\Omega} \frac{\partial \mathbf{N}^{\mathrm{T}}}{\partial \eta}\frac{B}{P}\frac{\partial \mathbf{N}}{\partial \xi}\,\mathrm{d}\Omega\right] \tag{A.9c}$$

$$\mathbf{C} = \int\int_{\Omega} \frac{\partial \mathbf{N}^{\mathrm{T}}}{\partial \eta}\frac{C}{P}\frac{\partial \mathbf{N}}{\partial \eta}\,\mathrm{d}\Omega \tag{A.9d}$$

$$\mathbf{D} = \int\int_{\Omega} \mathbf{N}^{\mathrm{T}}\left(\frac{1}{2}\frac{\partial(B/P)}{\partial \eta} + \frac{\partial(A/P)}{\partial \xi} - \frac{D}{P}\right)\frac{\partial \mathbf{N}}{\partial \xi}\,\mathrm{d}\Omega \tag{A.9e}$$

$$\mathbf{E} = \int\int_{\Omega} \mathbf{N}^{\mathrm{T}}\left(\frac{1}{2}\frac{\partial(B/P)}{\partial \xi} + \frac{\partial(C/P)}{\partial \eta} - \frac{E}{P}\right)\frac{\partial \mathbf{N}}{\partial \eta}\,\mathrm{d}\Omega \tag{A.9f}$$

Appendix B

Navier–Stokes equations:

$$\begin{aligned}
&\frac{\mathrm{D}u}{\mathrm{D}t} + \mathbf{u}\cdot\nabla u - \frac{\mathrm{d}\mathbf{x}}{\mathrm{d}t}\cdot\nabla u - \nabla^{\mathrm{T}}\left(\frac{\mu}{\rho_0}\nabla u\right) \\
&\quad - \frac{\lambda}{\rho_0}\frac{\partial}{\partial x}\left(\frac{\partial u}{\partial x} + \frac{\partial v}{\partial y}\right) = 0 \\
&\frac{\mathrm{D}v}{\mathrm{D}t} + \mathbf{u}\cdot\nabla v - \frac{\mathrm{d}\mathbf{x}}{\mathrm{d}t}\cdot\nabla v - \nabla^{\mathrm{T}}\left(\frac{\mu}{\rho_0}\nabla v\right) \\
&\quad - \frac{\lambda}{\rho_0}\frac{\partial}{\partial y}\left(\frac{\partial u}{\partial x} + \frac{\partial v}{\partial y}\right) = \frac{(\rho_0-\rho)g}{\rho_0}
\end{aligned} \tag{B.1}$$

Finite element approximation (on an element level):

$$\mathbf{C}_V\begin{Bmatrix} \frac{\partial \mathbf{u}}{\partial t} \\ \frac{\partial \mathbf{v}}{\partial t} \end{Bmatrix} + (\mathbf{K}_V + \mathbf{U}_V + \mathbf{L}_V)\begin{Bmatrix} \mathbf{u} \\ \mathbf{v} \end{Bmatrix} = \begin{Bmatrix} \mathbf{F}_x \\ \mathbf{F}_y \end{Bmatrix} \tag{B.2}$$

$$\mathbf{C}_V = \begin{bmatrix} \int\int_{\Omega}\mathbf{N}^{\mathrm{T}}\mathbf{N}\,\mathrm{d}\Omega & 0 \\ 0 & \int\int_{\Omega}\mathbf{N}^{\mathrm{T}}\mathbf{N}\,\mathrm{d}\Omega \end{bmatrix} \tag{B.3}$$

$$\mathbf{K}_V = \begin{bmatrix} \int\int_{\Omega}\frac{\mu}{\rho_0}\left(\frac{\partial \mathbf{N}^{\mathrm{T}}}{\partial x}\frac{\partial \mathbf{N}}{\partial x} + \frac{\partial \mathbf{N}^{\mathrm{T}}}{\partial y}\frac{\partial \mathbf{N}}{\partial y}\right)\mathrm{d}\Omega & 0 \\ 0 & \int\int_{\Omega}\frac{\mu}{\rho_0}\left(\frac{\partial \mathbf{N}^{\mathrm{T}}}{\partial x}\frac{\partial \mathbf{N}}{\partial x} + \frac{\partial \mathbf{N}^{\mathrm{T}}}{\partial y}\frac{\partial \mathbf{N}}{\partial y}\right)\mathrm{d}\Omega \end{bmatrix} \tag{B.4}$$

$$\mathbf{U}_V = \begin{bmatrix} \int\int_{\Omega}\mathbf{N}^{\mathrm{T}}\left(u\frac{\partial \mathbf{N}}{\partial x} + v\frac{\partial \mathbf{N}}{\partial y}\right)\mathrm{d}\Omega & 0 \\ 0 & \int\int_{\Omega}\mathbf{N}^{\mathrm{T}}\left(u\frac{\partial \mathbf{N}}{\partial x} + v\frac{\partial \mathbf{N}}{\partial y}\right)\mathrm{d}\Omega \end{bmatrix} \tag{B.5}$$

$$\mathbf{L}_V = \frac{\lambda}{\rho_0}\begin{bmatrix} \int\int_{\Omega}\frac{\partial \mathbf{N}^{\mathrm{T}}}{\partial x}\frac{\partial \mathbf{N}}{\partial x}\,\mathrm{d}\Omega & \int\int_{\Omega}\frac{\partial \mathbf{N}^{\mathrm{T}}}{\partial x}\frac{\partial \mathbf{N}}{\partial y}\,\mathrm{d}\Omega \\ \int\int_{\Omega}\frac{\partial \mathbf{N}^{\mathrm{T}}}{\partial y}\frac{\partial \mathbf{N}}{\partial x}\,\mathrm{d}\Omega & \int\int_{\Omega}\frac{\partial \mathbf{N}^{\mathrm{T}}}{\partial y}\frac{\partial \mathbf{N}}{\partial y}\,\mathrm{d}\Omega \end{bmatrix} \tag{B.6}$$

$$\begin{Bmatrix} \mathbf{F}_x \\ \mathbf{F}_y \end{Bmatrix} = \begin{Bmatrix} \int\int_{\Omega}\mathbf{N}^{\mathrm{T}}\frac{\mathrm{d}\mathbf{x}}{\mathrm{d}t}\cdot\nabla u\,\mathrm{d}\Omega \\ \int\int_{\Omega}\mathbf{N}^{\mathrm{T}}\left[\frac{(\rho_0-\rho)g}{\rho_0} + \frac{\mathrm{d}\mathbf{x}}{\mathrm{d}t}\cdot\nabla v\right]\mathrm{d}\Omega \end{Bmatrix} \tag{B.7}$$

Notes:

(i) First only element matrices $\mathbf{K}_V$ and $\mathbf{U}_V$ are computed and assembled. Let z be the value of the maximum by absolute value element in the assembled matrix. Let p be the number of digits in the computer presentation of a real number. In order half of the significant digits of $\sum(\mathbf{K}_V + \mathbf{U}_V)$ to be preserved after assembling all $\mathbf{L}_V$, the penalty number λ is computed as $\lambda = \exp(\log(z) + p/2)$.

(ii) The global penalty matrix $\sum\mathbf{L}_V$ needs to be singular so matrices $\mathbf{L}_V$ are computed by reduced integration, one point Gauss quadrature.

(iii) For a fully solid element (one for which the maximum nodal temperature is less than the melting temperature, i.e. $\max T_N < T_{\mathrm{m}}$) the matrices in Eq. (30) are not computed. For a partially solid element (i.e. $\min T_N < T_{\mathrm{m}} < \max T_N$) an artificial viscosity $\mu_{\mathrm{solid}} = 1000\mu$ is used if the Gauss point is in a solid state.

(iv) All nodes for which $T < T_{\mathrm{m}}$ (i.e. they are in a solid state) are prescribed zero velocities, in addition to the boundary nodes with no-slip boundary conditions.

References

Beckett, G., Mackenzie, J.A., Robertson, M.L., 2001. A moving mesh finite element method for the solution of two-dimensional Stefan problems. J. Comput. Phys. 168, 500–518.

Beckett, G., Mackenzie, J.A., Ramage, A., Sloan, D.M., 2002. Computational solution of two-dimensional unsteady PDEs using moving mesh methods. J. Comput. Phys. 182, 478–495.

Braga, S.L., Viskanta, S., 1992. Effect of density extremum on the solidification of water on a vertical wall of a rectangular cavity. Exp. Therm. Fluid Sci. 5, 703–713.

Cao, W., Huang, W., Russell, R.D., 1999. An *r*-adaptive finite element method based upon moving mesh PDEs. J. Comput. Phys. 149, 221–244.

Crank, J., 1984. Free and Moving Boundary Problems. Clarendon Press, Oxford.

Crivelli, L.A., Idelsohn, S.R., 1986. A temperature-based finite element solution for phase-change problems. Int. J. Numer. Methods Eng. 23, 99–119.

Dalhuijsen, A.J., Segal, A., 1981. Comparison of finite techniques for solidification problems. Int. J. Numer. Methods Eng. 23, 81–96.

Fachinotti, V.D., Cardona, A., Huespe, A.E., 1999. A fast convergent and accurate temperature model for phase change heat conduction. Int. J. Heat Mass Transfer 44, 1863–1884.

Gobin, D., Le Quéré, P., 2000. Melting from an isothermal vertical wall. Synthesis of a numerical comparison. Comput. Assist. Mech. Eng. Sci. 7, 289–306.

Gupta, S.C., 2000. A moving grid numerical scheme for multidimensional solidification with transition temperature range. Comput. Methods Appl. Mech. Eng. 189, 525–544.

Hannoun, N., Alexiades, V., Mai, T.Z., 2003. Resolving the controversy over tin and gallium melting in a rectangular cavity heated from the side. Numer. Heat Transfer, Part B 44, 253–276.

Heinrich, J.C., Pepper, D.W., 1996. The Intermediate Finite Element Method. Taylor and Francis.

Huang, W., 1999. Practical aspects of formulation and solution of moving mesh partial differential equations. Mathematics Research Report No. 99-11-02, University of Kansas.

Lewis, R.W., Roberts, P.M., 1987. Finite element simulation of solidification problems. Appl. Sci. Res. 44, 61–92.

Lynch, D.R., 1985. Unified approach to simulation on deforming elements with application to phase change problems. J. Comput. Phys. 57, 303–317.

Lynch, D.R., O'Neill, K., 1981. Continuously deforming finite elements for the solution of parabolic problems with and without phase change. Int. J. Numer. Methods Eng. 17, 81–96.

Mackenzie, J.A., Robertson, M.L., 2000. The numerical solution of one-dimensional phase change problems using an adaptive moving mesh method. J. Comput. Phys. 161, 537–557.

Miller, K., Miller, R.N., 1981. Moving finite elements. SIAM J. Numer. Anal. 18, 1019–1057.

Morgan, K., Lewis, R.W., Zienkiewicz, O.C., 1978. An improved algorithm for heat conduction problems with phase change. Int. J. Numer. Methods Eng. 12, 1191–1195.

Nedjar, B., 2002. An enthalpy-based finite element method for nonlinear heat problems involving phase change. Comput. Struct. 80, 9–21.

Nigro, N., Huespe, A., Fachinotti, V., 2000. Phasewise numerical integration of finite element method applied to solidification processes. Int. J. Heat Mass Transfer 43, 1053–1066.

Ockendon, J.R., Hodgkins, W.R. (Eds.), 1975. Moving Boundary Problems in Heat Flow and Diffusion. Oxford University Press.

Pardo, E., Weckman, D.C., 1990. A fixed grid finite element technique for modeling phase change in steady state conduction–advection problems. Int. J. Numer. Methods Eng. 29, 969–984.

Rolph, W.D., Bathe, K.J., 1982. An efficient algorithm for analysis of nonlinear heat transfer with phase change. Int. J. Numer. Methods Eng. 18, 119–134.

Salcuden, M., Abdullah, Z., 1988. On the numerical modeling of heat transfer during solidification processes. Int. J. Numer. Methods Eng. 28, 445–473.

Scanlon, T.J., Stickland, M.T., 2004. A numerical analysis of buoyancy-driven melting and freezing. Int. J. Heat Mass Transfer 47, 429–436.

Tamma, K.K., Namburu, R.R., 1990. Recent advances, trends and new perspectives via enthalpy-based finite element formulations for applications to solidification problems. Int. J. Numer. Methods Eng. 30, 803–820.

Thomas, B.G., Samarasekara, I.V., Brimacombe, J.K., 1984. Comparison of numerical modeling techniques for complex two-dimensional, transient heat conduction problems. Metall. Trans. B 15, 307–318.

Voller, V., Cross, M., 1981. Accurate solutions of moving boundary problems using the enthalpy method. Int. J. Heat Mass Transfer 24, 545–556.

Voller, V.R., Swaminathan, C.R., Thomas, B.G., 1990. Fixed grid techniques for phase change problems: a review. Int. J. Numer. Methods Eng. 30, 875–898.